High-Temperature Oxidation of a Metal Particle: Nonisothermal Model

Igor Filimonov
Institute of Structural Macrokinetics and Materials Science RAS, Chernogolovka, 142432, Russia

Dan Luss
Dept. of Chemical Engineering, University of Houston, Houston, TX 77204

DOI 10.1002/aic.10393
Published online March 28, 2005 in Wiley InterScience (www.interscience.wiley.com).

A transient electric voltage of the order of 1 V may form during the combustion of a metal particle. The electrical field may form due to the different diffusion rate of the positive and negative charge carriers through a growing mixed-ionic-electronic conducting oxide shell. Unlike previous models, the effect of ambient gaseous oxygen transport to the particle surface is accounted for and steady-state and charge neutrality in the oxide layer is not a priori assumed. Four key parameters affect the voltage-temperature formation. The ratio between charge carries diffusion coefficients determines the surface electric potential amplitude, polarization and the time delay between the maximums of particle potential and temperature. The larger the difference between the diffusion coefficients, the greater is the voltage and the longer is the combustion time and the shorter is the time delay. The convection and radiation heat-transfer coefficients exert a major impact on the time delay between the maximum of the surface electric potential and that of the temperature. The maximum electric potential and temperature are achieved almost at the same time when the transport coefficients are sufficiently large. This time difference decreases as either the heat-transfer coefficients or the difference between the diffusion coefficients increase. Increasing the activation energy of the adsorption strongly decreased the oxidation, temperature and surface electric potential rate of rise during the early stage of the oxidation. Increasing the activation energy of the desorption increased the duration of the temperature and the potential drop in the later stage of the reaction.
© 2005 American Institute of Chemical Engineers *AIChE J,* 51: 1521–1531, 2005

Introduction

Recent experiments revealed that high-temperature oxidation of metal particles may generate a temporary voltage of the order of $1V$ [1-6]. The mechanism leading to the formation of this transient electrical field is not yet established. Metal particle oxidation may proceed in two ways, which depend on the metal properties and oxygen pressure. Metal cations (and/or their vacancies) may move and get oxidized at the particle surface (for example, *Fe* oxidation[7]), or oxygen ions (and/or their vacancies) may move to and react at the metal-oxide interface (for example, *Zr* oxidation[8]). The oxidation of some metals, like *Ti*, may occur either on the particle surface or on the metal-oxide interface depending on operating conditions[7,9,10]. The different diffusion velocities of the charge carriers through the oxide may form an electric potential across the growing oxide shell[11-13].

Previous models[11-13] of charge formation in a membrane or oxide layer assume that local electrochemical equilibrium, as well as electroneutrality exists in the layer between the moving

Correspondence concerning this article should be addressed to D. Luss at Dluss@uh.edu.

© 2005 American Institute of Chemical Engineers

pairs of positive and negative charge carriers. These models assume that the oxygen partial pressure at the oxide surface equals to the ambient oxygen partial pressure, that is, ignore the surface adsorption-desorption reactions and the external transport resistances. Thermoionic emission and electron tunneling[14] have been considered as the cause of electron transport through thin oxide films at elevated-temperature oxidation. "Single-current" models[14] assume that the oxide growth rate is limited by the flux of a limiting charge carrier and disregard the contribution from the second. Hence, they consider that oxide growth occurs only by ionic diffusion in very thin films ($\propto$10 Å) and only by electron transport in thicker films.

The "coupled-currents" approach[15-18] accounts for the simultaneous transport of several charge carriers and assumes that no net electric charge is transported through the oxide layer. This approach is adequate for low-temperature oxidation for which the oxidation proceeds at a quasi steady-state and its characteristic time is of the order of hours and days[15-18]. These models do not explain the electric field generation during a fast, high-temperature combustion, the characteristic time of which is of the order of a second or less[19-24,1-4].

We present here a model explaining the electrical field generation during the high-temperature oxidation of a spherical metal particle. It predicts for the dependence of the electric field on the oxygen chemical adsorption and desorption on the particle surface, as well as on the temporal difference in the rate of movement of formed charge carriers through the growing oxide shell. The impact of the temperature rise during the exothermic reaction is revealed by comparing the predictions for the nonisothermal case with our previous ones for the isothermal case[25]. The qualitative model predictions are compared with experimental results.

Mathematical model

We consider the high-temperature oxidation of a spherical metal particle of radius R_0. The reaction occurs at the metal-oxide interface, that is, the oxide is a mixed-ionic-electronic-conductor (MIEC). The model can be readily modified to the case, in which the oxidation proceeds at the particle surface and the oxide layer is a semiconductor. We assume that the rate of the metal oxidation is very fast relative to the ion diffusion rate so that the oxide shell growth can be described by the shell progressive model[26,27]. The ambient gaseous oxygen is adsorbed on the pellet surface via the reversible reaction

$$O_2(g) \underset{k'_{-1}}{\overset{k_1}{\rightleftarrows}} 2O_{ads}. \tag{1}$$

The adsorbed oxygen forms lattice atoms, as well as interstitial ions and vacancies in the oxide lattice by the reactions

$$V_O^{++} + 2e^- + O_{ads} \underset{k'_{-2}}{\overset{k'_2}{\rightleftarrows}} O^{\times} \underset{k'_{-3}}{\overset{k'_3}{\rightleftarrows}} V_O^{++} + O^{2-} \tag{2}$$

Simultaneously, electron-hole pairs are generated via thermal ionization

$$nil \underset{k'_{-4}}{\overset{k'_4}{\rightleftarrows}} e^- + h^+ \tag{3}$$

The different diffusion rates of the charge carriers (V_O^{++}, e^- and O^{2-}, h^+) generate an electric charge in the growing oxide shell. The oxygen ions and electron holes are consumed by a very fast, irreversible reaction at the shrinking metal core (radius R_{ox})

$$\nu Me + 2O^{2-} + 4h^+ \rightarrow Me_\nu O_2 \tag{4}$$

We assume that the temperature within the particle is uniform, but different from the ambient gas, and that neither melting nor phase transformations occur. The reaction network 1–3 is a generalization of that for solid oxide electrolytes with mixed electronic-ionic conductivity[28-30,8]. The reaction rates satisfy the relations

$$W_1 = -\frac{1}{2}\frac{d[O_{2,g}]'}{dt} = k_1[O_{2,g}]^{1/2} - k'_{-1}[O_{ads}] \tag{5}$$

$$W_2 = \frac{d[O^{\times}]'}{dt} = -\frac{d[V_O^{++}]'}{dt} = k'_2[V_O^{++}]\cdot[e^-]^2[O_{ads}] - k'_{-2}[O^{\times}] - k'_3[O^{\times}] + k'_{-3}[V_O^{++}][O^{2-}] \tag{6}$$

$$W_3 = \frac{d[O^{2-}]'}{dt} = k'_3[O^{\times}] - k'_{-3}[V_O^{++}][O^{2-}] \tag{7}$$

$$W_4 = -\frac{d[h^+]'}{dt} = k'_4 - k'_{-4}[e^-]\cdot[h^+] \tag{8}$$

The lattice oxygen concentration $[O^{\times}]'$, may be assumed to be a constant in the MIEC shell[30,8]. In addition, we assume that the concentrations of the interstitial oxygen ions (O^{2-}) and electron holes (h^+) attain a quasi-steady state, that is

$$W_i = 0, \quad i = 2, 3, 4 \tag{9}$$

The oxygen concentration near the pellet surface $[O_{2,g}]$, satisfies the relation

$$W_1 = k_c([O_{2,g}]^{\infty} - [O_{2,g}]) \tag{10}$$

where k_c is the mass-transfer coefficient and $[O_{2,g}]^{\infty}$ is the ambient oxygen concentration.

At a high oxygen pressure interstitial oxygen ions (O^{2-}) and electron holes (h^+) are the main contributors to oxygen and electrical charge transport in MIEC materials[30,31,8]. Equations 6–9 indicate that in this case

$$[O^{2-}]\cdot[h^+]^2 = \frac{k'_{-1}}{k_{-1}}\cdot[O_{ads}], \quad k_{-1} = k'_{-1}\left(\frac{k'_{-2}}{k'_2}\right)\left(\frac{k'_{-3}}{k'_3}\right)\left(\frac{k'_{-4}}{k'_4}\right)^2. \tag{11}$$

The electrochemical equilibrium concentrations of reactions 1–3 at the reference temperature T^*, chosen as the adiabatic temperature rise due to oxidation ($T^* = (-\Delta H)/(\rho_{cond} C)$), are

$$[O^{2-}]^* = \left(\frac{k_1(T^*)}{4k_{-1}(T^*)}\right)^{1/3} ([O_{2,g}]^\infty)^{1/6},$$

$$[h^+]^* = \left(\frac{2k_1(T^*)}{k_{-1}(T^*)}\right)^{1/3} ([O_{2,g}]^\infty)^{1/6} \quad (12)$$

Oxygen ion vacancies (V_O^{++}) and electrons (e^-) are the main source of oxygen permeation through the membranes at low oxygen pressures and

$$[V_O^{++}]^{-1}[e^-]^{-2} = \frac{k'_{-1}}{\tilde{k}_{-1}}[O_{ads}], \quad \tilde{k}_{-1} = k'_{-1}\left(\frac{k'_{-2}}{k'_2}\right)[O^\times] \quad (13)$$

The electrochemical equilibrium concentrations of reactions 1–3 at T^* are

$$[V_O^{++}]^* = \left(\frac{\tilde{k}_{-1}(T^*)}{4k_1(T^*)}\right)^{1/3} ([O_{2,g}]^\infty)^{-1/6},$$

$$[e^-]^* = \left(\frac{2\tilde{k}_{-1}(T^*)}{k_1(T^*)}\right)^{1/3} ([O_{2,g}]^\infty)^{-1/6} \quad (14)$$

We consider operation conditions for which $[O_{2,g}]^\infty \gg k_{-1}\tilde{k}_{-1}/k_1^2$, so that

$$[O^{2-}]^* \gg [V_O^{++}]^*, \quad [h^+]^* \gg [e^-]^*. \quad (15)$$

The inverse of inequality (Eq. 15) is valid at low oxygen concentrations. At intermediate oxygen concentrations, one has to account for all four charge carriers (oxygen ions, vacancies, holes and electrons). Solving Eqs. 5, 10, and 11 we get

$$y = \frac{A(\theta)^2}{4}\left(\left[1 + \frac{4}{A(\theta)^2} + \frac{4\cdot\chi\cdot np^2}{A(\theta)}\right]^{1/2} - 1\right)^2 \quad (16)$$

where

$$y = [O_{2,g}]/[O_{2,g}]^\infty, \quad n = [O^{2-}]/[O^{2-}]^*,$$

$$p = [h^+]/[h^+]^*, \quad \theta = T/T^* \quad (17)$$

$$\gamma_1 = \frac{E_1}{RT^*}, \quad \gamma_{-1} = \frac{E_{-1}}{RT^*}, \quad k_i(\theta) = k_i^0\cdot\exp(-\gamma_i/\theta), \quad i = +1, -1$$

$$\chi = \frac{k_1(1)}{k_1(\theta)}\frac{k_{-1}(\theta)}{k_{-1}(1)} = \exp\left\{(\gamma_{-1} - \gamma_1)\cdot\left(1 - \frac{1}{\theta}\right)\right\}$$

$$A_0 = \frac{k_1(1)}{k_c([O_{2,g}]^\infty)^{1/2}}, \quad A = A_0\exp\left\{\gamma_1\left(1 - \frac{1}{\theta}\right)\right\}$$

It predicts that no oxygen adsorption occurs ($y \to 1$) either at low-temperatures ($A \to 0$), or when the reaction is completed and the surface carrier concentrations tend to the equilibrium values ($n \to \chi^{-1/3}$, $p \to \chi^{-1/3}$). According to Eq. 17 the difference in the activation energies of the adsorption and desorption rate constants determines the behavior of the surface carrier concentrations at the later stages of the combustion, when these concentrations tend to equilibrium and the temperature drops. For $\gamma_{-1} < \gamma_1$ the concentrations decrease as the temperature decreases ($\theta < 1$) and vice versa for $\gamma_{-1} > \gamma_1$.

The steady-state nondimensional boundary conditions are

$$\beta\cdot\left(\nabla_\xi n - 2\frac{n}{\theta}\nabla_\xi\phi\right)_{\xi=1} = 1 - y \quad \text{at } \xi = 1 \quad (18)$$

$$\bar{D}\cdot\beta\cdot\left(\nabla_\xi p + \frac{p}{\theta}\nabla_\xi\phi\right)_{\xi=1} = 1 - y \quad \text{at } \xi = 1 \quad (19)$$

where

$$\bar{D} = D_+/D_-, \quad \xi = r/R_0, \quad \phi = e\varphi/kT^* \quad (20)$$

$$\beta = \left(\frac{D_-[O^{2-}]^*}{2R_0}\right)\Big/(k_c[O_{2,g}]^\infty)$$

The electric potential distribution satisfies the Poisson equation

$$\Lambda^2\cdot\Delta_{\xi\xi}\phi - n + p = 0, \quad \Lambda = \left\langle\frac{kT_0}{4\pi\cdot e^2}\frac{1}{R_0^2}\frac{1}{[h^+]^* N_A}\right\rangle^{1/2} \quad (21)$$

The charge carrier distributions within the oxide shell satisfy the transient diffusion equations

$$\frac{\partial n}{\partial\tau} = \nabla_\xi^2 n - 2\nabla_\xi\left(\frac{n}{\theta}\nabla_\xi\phi\right) \quad (22)$$

$$\frac{\partial p}{\partial\tau} = \bar{D}\cdot\left\{\nabla_\xi^2 p + \nabla_\xi\left(\frac{p}{\theta}\nabla_\xi\phi\right)\right\} \quad (23)$$

where

$$\tau = t\cdot D_-/R_0^2$$

The Poisson-Nernst-Plank equations[32-34] are the steady state version of Eq. 21-23. The electric potential within the shrinking core is uniform due to the high metal conductivity. Thus

$$\left(\frac{\partial\phi}{\partial\xi}\right) = 0, \quad \xi = \xi_{ox} \quad (24)$$

Charge conservation at the particle surface is a boundary condition, that is

$$\left(\frac{\partial\phi}{\partial\xi}\right) = p - n, \quad \xi = 1 \quad (25)$$

The charge carriers are consumed by a very fast, irreversible reaction at the shrinking metal core (metal-oxide interface), that is

$$n = p = 0, \quad \xi = \xi_{ox} > 0 \tag{26}$$

When all the metal has been oxidized, this boundary condition is replaced by

$$\frac{\partial n}{\partial \xi} = \frac{\partial p}{\partial \xi} = 0, \quad \xi \equiv 0. \tag{27}$$

The molar consumption rate of the metal is $\nu/2$ of that of the oxygen ions. Thus

$$\frac{d\xi_{ox}}{d\tau} = -I \cdot \beta \left(\nabla_{\xi} n - \frac{2n}{\theta} \nabla_{\xi} \phi \right)_{\xi = \xi_{ox}}, \quad I = \frac{\nu}{2} \frac{M_W}{\rho} [O_{2,g}]^{\infty} \left(\frac{2k_c R_0}{D_-} \right) \tag{28}$$

The dimensionless thermal balance is

$$\frac{d\theta}{d\tau} = -3\xi_{ox}^2 \frac{d\xi_{ox}}{d\tau} + H_0 \int_0^1 (\xi \nabla_{\xi} \phi)^2 d\xi - H_1(\theta - \theta_{00}) - H_2(\theta^4 - \theta_{00}^4) \tag{29}$$

where

$$H_0 = 3 \left(\frac{k}{C \rho_{cond} \cdot e} \right)^2 \frac{\sigma_{el}(-\Delta H)}{D_-}, \quad H_1 = \frac{\alpha}{C \rho_{cond}} \frac{3R_0}{D_-}, \quad H_2 = \frac{\varepsilon \sigma}{(C \rho_{cond})^4} \cdot (-\Delta H)^3 \frac{3R_0}{D_-} \tag{30}$$

The terms on the rhs of Eq. 29 account for the chemical reaction, Joule dissipation, thermal convection and radiation, respectively. The temperature rise by Joule dissipation is negligibly small during gas-solid combustion reactions[24] and is ignored, that is, we assume $H_0 = 0$. The model consists of Eqs. 21–23 subject to boundary conditions Eqs. 18, 19, 26, and 27 for the carrier concentrations, and Eqs. 24, 25 for the electric potential. Ordinary differential Eqs 28 and 29 describe the changes in ξ_{ox} and θ. The initial conditions are

$$n = p = \phi \equiv 0, \quad \theta = \theta_0 \quad \text{at} \quad \tau = 0, \ \forall \xi \tag{31}$$

The elliptic Eq. 21 was treated as a parabolic one using the relaxation method[35] with a very small time constant ($\bar{\varepsilon} = 10^{-4}$). It was integrated simultaneously with the others by the method of finite differences. The equations were transformed into a tridiagonal set of linear algebraic equations and integrated using the Crank and Nicholson method[36] with a uniform finite differences grid (up to 500 nodes). These were solved by the Thomas algorithm[37,38].

Numerical results

We used numerical simulations to study the evolution of the electric charge carriers, temperature and temporal potential distribution during the high-temperature oxidation of a single metal particle. We assume that initially the particle is heated to a temperature at which the intrinsic chemical reaction rate greatly exceeds that of the carrier diffusion. Thus, the shrinking core model adequately describes the metal oxidation rate. We assume that neither melting nor phase transformation occurs during the reaction. Our goal is to gain an understanding about the evolution of an electric voltage during the metal oxidation, and the relation between the particle temperature rise and the temporal electric potential formation. This information will enable a critical test of the validity of the model assumptions.

The simulations indicate that the dimensionless parameters that most strongly affect the temperature and evolution of the electric potential are: the ratio between the diffusion coefficients of the two charge carriers ($\bar{D}$), which is considered as the exponential function of temperature $\bar{D} = \bar{D}_0 \exp(E_{\bar{D}}/\theta)$, the ratio between a characteristic surface molar flux of oxygen ions to the maximum possible oxygen flux to the pellet surface (β), the heat removal coefficients (H_1 and H_2) as well as the activation energy of adsorption (γ_1) and the difference between the activation energies of desorption and adsorption ($\gamma_{-1} - \gamma_1$). Usually, a thin oxide shell forms before the shell progressive reaction starts and the thickness of that shell affects the voltage formation. We do not investigate here the influence of an initial oxide shell thickness (ξ_{ox}^0) , as well as that of the initial (θ_0) and surrounding temperatures (θ_{00}). These will be considered in a future publication. We assume in all the simulations that $\xi_{ox}^0 = 0.994$, $\theta_0 = 0.5$, $\theta_{00} = 0.15$, $\Lambda = 0.01$, $A_0 = 10^5$ and $I = 21.3$.

The main available experimental data about metal particles combustion are the temporal evolution of the voltage, current and temperature, as well as the time of complete combustion. A critical test of the validity of the underlying model assumptions can be done by comparing its predictions with data about the time difference at which the maximum voltage and temperatures are attained. We study this difference to enable this comparison.

Figure 1 describes the influence of $\bar{D}$ (θ) on the charge carrier distributions during the oxidation of a single particle with a thin initial oxide shell ($1 - \xi_{ox}^0$) $\ll \Lambda$. In general, there are four qualitative types of $\bar{D}(\theta)$ behavior during the initial temperature rise to the maximum temperature. They depend on the pre-exponential coefficient $\bar{D}_0$, and the difference in the activation energies of the diffusion coefficients $E_{\bar{D}}$. We consider here only the two simplest ones: when $\bar{D}(\theta) > 1$ at $\theta_0 < \theta < \theta_m$ and when $\bar{D}(\theta) < 1$ at $\theta_0 < \theta < \theta_m$. The other two are the intermediate cases, for which $\bar{D}(\theta) - 1$ changes sign in $\theta_0 < \theta < \theta_m$. Simulations show that $\bar{D}$ (θ) has a negligible influence on the charge carrier distributions and potential after $\theta = \theta_m$ is attained, and the surface carrier concentrations are very close to each other and to the equilibrium concentrations. The profiles of the positive and negative charge carriers are almost identical throughout the particle so that the electrical charge in the shrinking metal core and in most of the oxide shell is negligibly small. A noticeable difference between the p and n concentrations and an electric charge exists close to the particle surface for a short initial period $\tau < \tau|_{\theta_m}$. The differ-

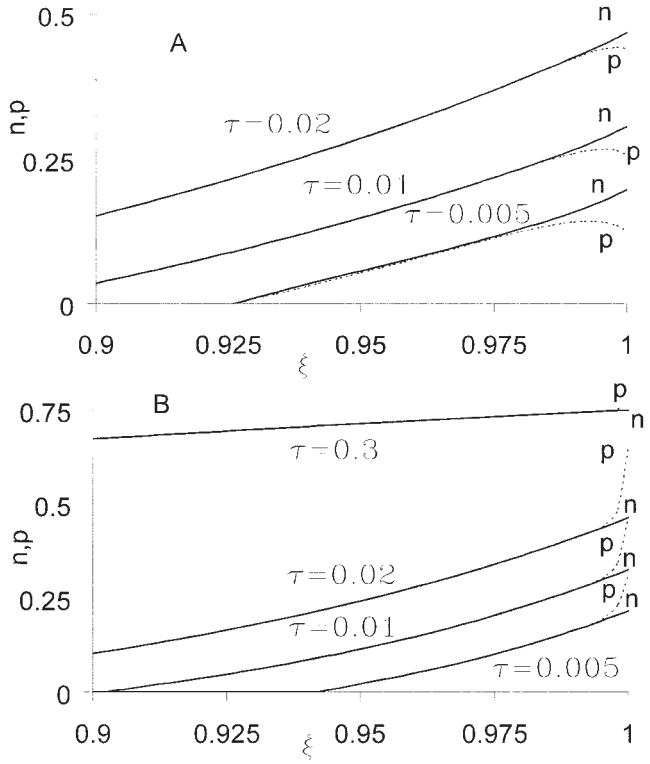

Figure 1. Dependence of the spatial distribution of the charge carriers on $\bar{D}$ during the first stage of oxidation of a pellet with a thin initial oxide shell: $\bar{D}_0 = 0.01$, $\beta = 0.2$, $\gamma_1 = 8$, $\gamma_{-1} = 5$, $H_1 = 1.72$, $H_2 = 0.967$, $E_{\bar{D}} = 5$(a), $E_{\bar{D}} = 2$(b)

ence is a monotonic increasing function of $|\bar{D}(\theta) - 1|$ during this period. The difference initially decreases with temperature rise at large $E_{\bar{D}}$ ($\bar{D}(\theta) > 1$, Figure 1a) or increases at small $E_{\bar{D}}$ ($\bar{D}(\theta) < 1$, Figure 1b). When the ratio between the positive and negative diffusion coefficient $\bar{D}$ (θ) exceeds unity, $n > p$ close to the surface ($\xi \rightarrow 1$, Figure1a), while the inverse occurs when $\bar{D}$ (θ) < 1 (Figure 1b). This difference between the surface p and n concentrations vanishes rapidly with time ($\tau \rightarrow 1$) (Figure 1b). In most cases n and p become almost indistinguishable when $\tau \approx 1$. The n, p profiles are weakly dependent on $\bar{D}$ after the initial period.

Figures 2 and 3 illustrate the effect of the $\bar{D}$ (θ) ratio on the temporal combustion characteristics and amplitudes. Figures 2a and 3a show that both $\bar{D}_0$ and $E_{\bar{D}}$ have a negligible impact on the maximum combustion temperature. However, ϕ_m and the maximum potential difference across the shell $\Delta\phi_m$, strongly depend on both $\bar{D}_0$ and $E_{\bar{D}}$ (Figures 2a and 3a). When the diffusion coefficients of the two charge carriers are equal $\bar{D}$ (θ_0) $= 1$ and $E_{\bar{D}} = 0$, no potential forms, that is, $\phi = 0$ (Figure 3a). The surface electric potential changes from positive to negative when $\bar{D}$ (θ_0) $= 1$. The amplitudes of ϕ_m and $\Delta\ \phi_m$ increase with $|\bar{D}(\theta_0) - 1|$.

The time of complete metal oxidation (τ_c) and that at which the maximum temperature is attained ($\tau|_{\theta_m}$) decrease monotonically, while the positive difference of $\tau_c - \tau|_{\phi_m}$ decreases when either $\bar{D}_0$ or $E_{\bar{D}}$ increases (Figures 2b and 3b). Similarly, the time at which the maximum surface electric potential is achieved, $\tau|_{\phi_m}$, increases, while the positive difference $\tau|_{\theta_m} - \tau|_{\phi_m}$ decreases when either $\bar{D}_0$ or $E_{\bar{D}}$ increases. The maximums of the temperature and surface electric potential converge and tend to be attained closer to the time of complete metal oxidation ($\eta|_{\tau_c} \equiv 1$) with increasing $\bar{D}_0$ or $E_{\bar{D}}$. The conversion at the maximum temperature $\eta|_{\theta_m}$, weakly increases and always $\eta|_{\theta_m} < \eta|_{\tau_c} \equiv 1$ as either $\bar{D}_0$ or $E_{\bar{D}}$ increase. The conversion at the maximum surface electric potential $\eta|_{\phi_m}$, drastically increases and becomes 5–10 times larger with increasing $\bar{D}_0$ or $E_{\bar{D}}$ (Figures 2b and 3b).

Figure 4 describes the influence of the convective heat transfer coefficient H_1 while Figure 5 that of the radiation heat-transfer coefficient H_2. In the cases shown in these two figures, the maximum surface electric potential, and the corresponding time and conversion ($\eta|_{\phi_m}$), are independent of H_1 or H_2. However, the maximum temperature decreases with an increase in either H_1 or H_2. The time at which the maximum temperature θ_m is achieved $\tau|_{\theta_m}$, and the corresponding conversion $\eta|_{\theta_m}$, smoothly decrease as H_1 increases. However, their values sharply drop when $0 \leq H_2 <\cong 5$, and very moderately when $H_2 \geq 5$ (Figures 4 and 5). The time of complete metal oxidation decreases gradually with an increase in either H_1 or H_2 and in all cases $\tau|_{\phi_m} < \tau|_{\theta_m} < \tau_c$. The difference between the times at which the electric signal and temperature attains their maximum $\tau|_{\theta_m} - \tau|_{\phi_m}$, sharply declines as H_1 or H_2 increases (Figures 4 and 5).

Figure 6 shows that an increase in the activation energy of the adsorption decreases the temporal temperature and conversion and increases the time at which the maximum surface

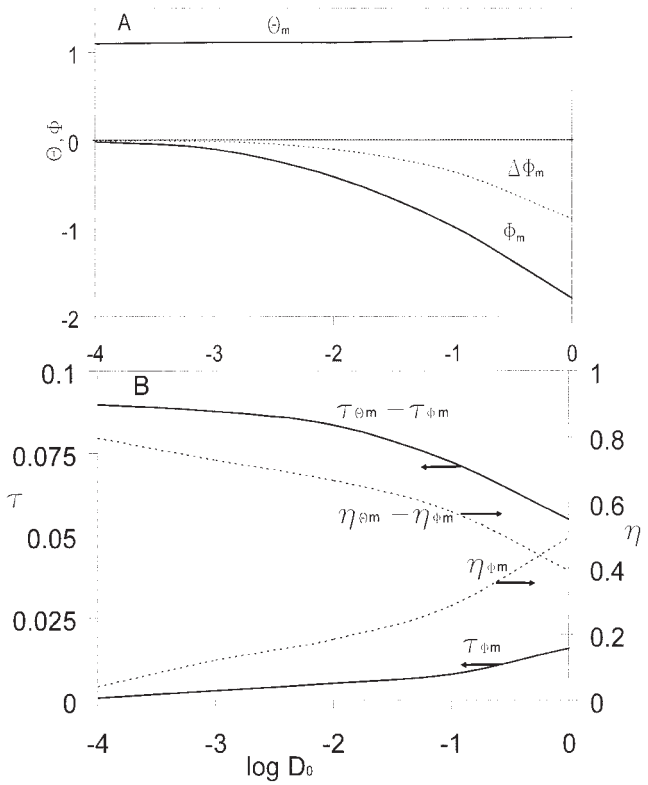

Figure 2. Dependence of the maximum temperature and maximum electric potential and their characteristics on : $\bar{D}_0$: $E_{\bar{D}} = 5$, $\beta = 0.5$.

The values of γ_1, γ_{-1}, H_1 and H_2 same as in Figure 1.

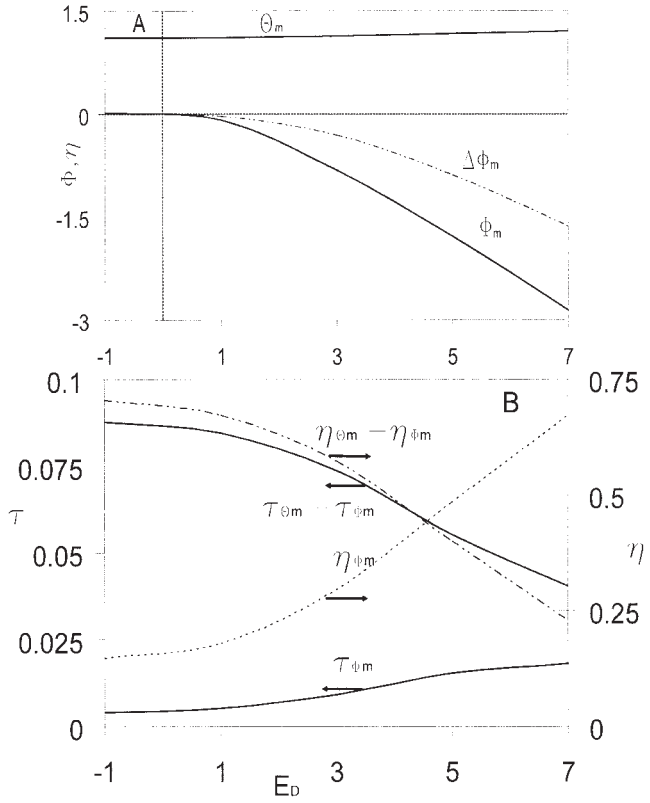

Figure 3. Dependence of the maximum temperature and maximum electric potential and their characteristics on : $E_{\bar{D}}$: $\bar{D}_0$ = 1.

The values of γ_1, γ_{-1}, β, H_1 and H_2 same as in Figure 2.

electric potential is attained (Figure 6b). All these events occur before the maximum particle temperature is achieved. The changes are more pronounced at higher values of H_1 or H_2 (Figure 6b). In contrast, increasing the activation energy of the desorption increases the temporal temperature, metal conversion (η) and the surface electric potential after the maximum

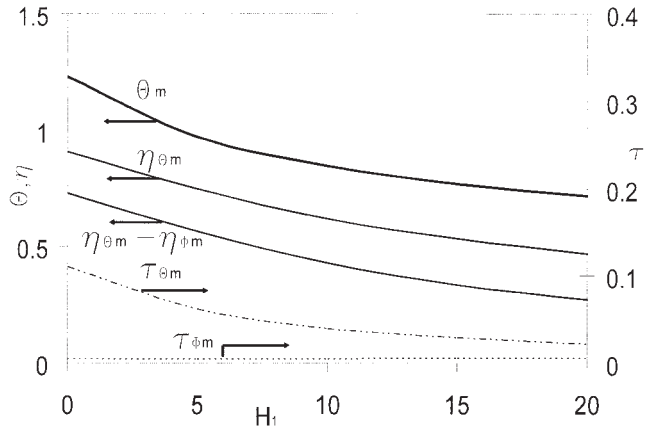

Figure 4. Dependence of the maximum temperature, maximum electric potential and their characteristics on : H_1: $\bar{D}_0$ = 0.01, $E_{\bar{D}}$ = 5.

The values of γ_1, γ_{-1}, β, and H_2 same as in Figure 2.

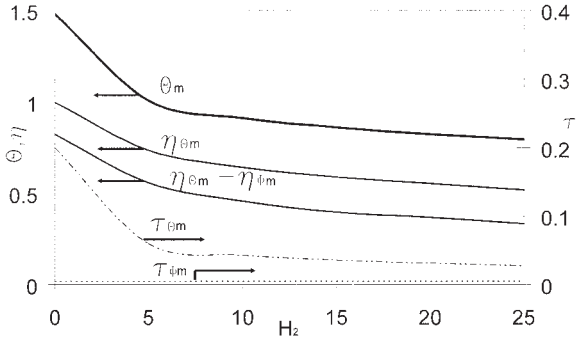

Figure 5. Dependence of the maximum temperature, maximum electric potential and their characteristics on H_2: $\bar{D}_0$ = 0.01, H_1 = 0, $E_{\bar{D}}$ = 5.

The values of γ_1, γ_{-1} and β, same as in Figure 2.

particle temperature and surface potential have been attained (Figure 7). The effect is more dominant at large H_1 or H_2 values.

The difference between the activation energies of the adsorption and desorption ($\gamma_{-1} - \gamma_1$), has a very small impact on the temporal temperature (Figure 8 and 9), surface potential and carrier distribution during the oxidation of a single particle with a thin initial oxide shell. The difference has some effect after the maximum temperature is attained. Thus, it does not affect the measurable difference between the times at which the maximum voltage and temperature are attained. The difference of ($\gamma_{-1} - \gamma_1$) determines at each temperature the equilibrium carrier concentrations, that is, the concentrations, that would be established in the particle if the combustion is suddenly interrupted and the temperature remains constant. As the temporal

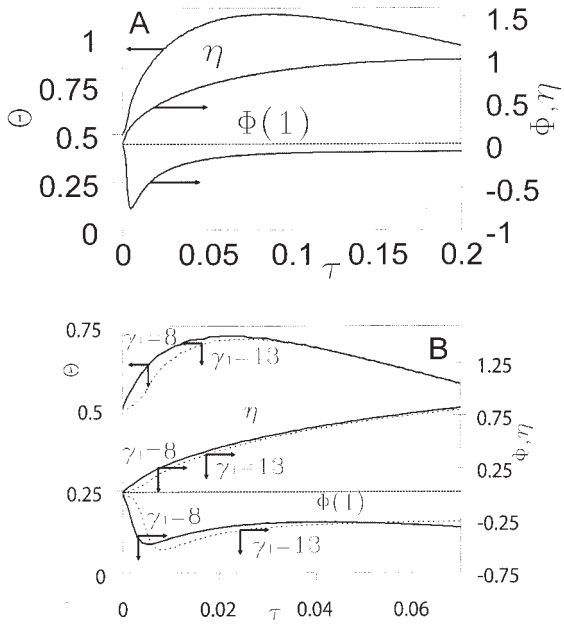

Figure 6. Effect of the activation energy of adsorption on the pellet temporal temperature, oxide volume and the surface electric potential : $\bar{D}_0$ = 0.01, $E_{\bar{D}}$ = 5, β = 0.2, γ_{-1} = 5, H_1 = 1.72 (a) or H_1 = 20. (b) H_2 = 0.967

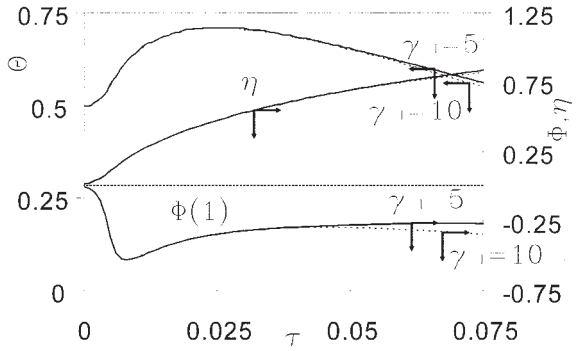

Figure 7. Effect of the activation energy of desorption on the pellet temporal temperature, oxide volume and the surface electric potential: $\bar{D}_0 = 0.01$, $E_{\bar{D}} = 5$, $\beta = 0.2$, $\gamma_1 = 13$, $H_1 = 20$, $H_2 = 0.967$.

particle temperature changes with time so do the temporal equilibrium concentrations of the carriers. They have a local minimum if $\gamma_{-1} - \gamma_1 > 0$ (Figure 8), and a local maximum if $\gamma_{-1} - \gamma_1 < 0$ (Figure 9), when the maximum temperature is achieved. The temporal equilibrium carrier concentrations are constant when the adsorption and desorption activation energies are equal ($\gamma_{-1} - \gamma_1 = 0$, in Figures 8 and 9). The concentrations of the charge carriers in a reacting particle approach the equilibrium values with time. The surface carrier concentrations become very close to the equilibrium values by the time of the maximum temperature has been achieved (Figures 8 and 9). According to the calculations the carrier concentrations on the metal-oxide interface need a much longer time to reach equilibrium and deviate from equilibrium until almost the end of the particle cooling.

An increase in the ratio between the characteristic surface molar flux of oxygen ions to the maximum possible oxygen flux to the particle surface,β, increases the values of ϕ_m and $\Delta\phi_m$, and has a minor impact on the combustion time τ_c (Figure 10). However, it has no impact on the temperature, time and

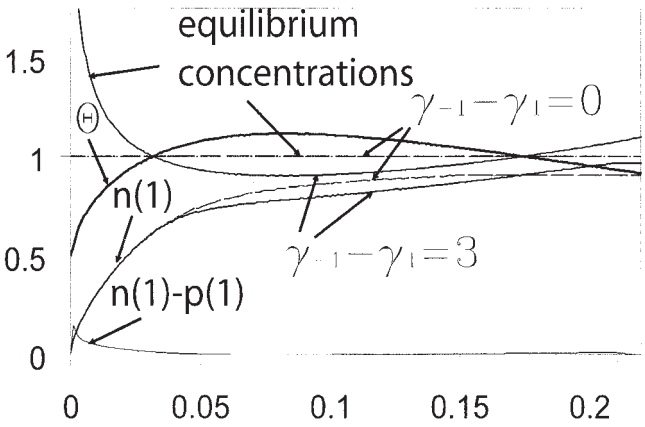

Figure 8. Dependence of the temporal actual and equilibrium concentrations of the charge carriers on the difference between the activation energies of adsorption and desorption at $\gamma_{-1} - \gamma_1 \geq 0$: $\bar{D}_0 = 0.01$, $E_{\bar{D}} = 5$.

The values of γ_1, β, H_1 and H_2, same as in Figure 1.

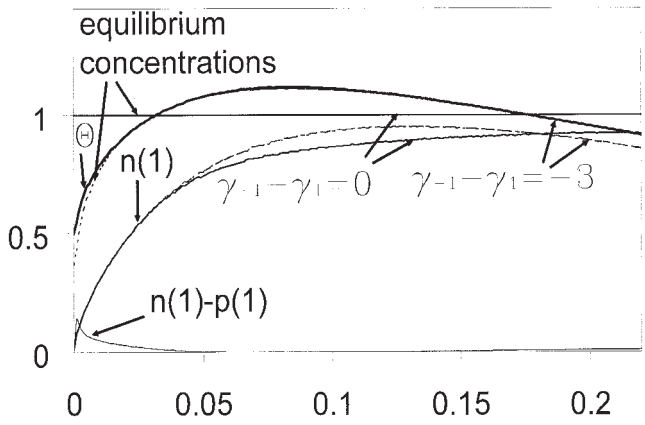

Figure 9. Dependence of the temporal actual and equilibrium concentrations of the charge carriers on the difference between the activation energies of adsorption and desorption at $\gamma_{-1} - \gamma_1 \leq 0$: $\bar{D}_0 = 0.01$, $E_{\bar{D}} = 5$.

The values of γ_1, β, H_1 and H_2, same as in Figure 1.

conversion at which either the maximum temperature or the maximum electric potential are achieved.

Discussion

The goal of this study was to enhance our understanding of the rate processes and parameters leading to the electric charge formation during the high-temperature oxidation of single metal particles. To gain that insight, we made the simplifying assumption that the reaction rate can be described by the shrinking core model. This implies that the characteristic reaction time at the metal-oxide interface is much shorter than that of ion diffusion. To check this we note that the characteristic time of the intrinsic metal oxidation t_r is of the order of 1 ms at 500°C[39]. The diffusion time of oxygen atoms at the same

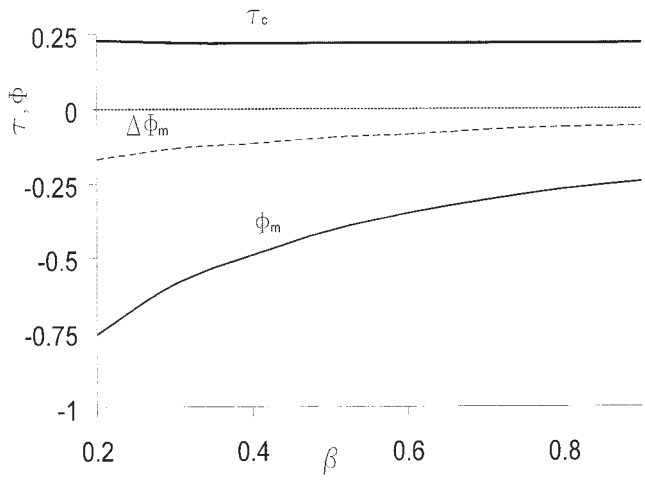

Figure 10. The dependence of the combustion time and surface electric potential on β: $\bar{D}_0 = 0.01$, $E_{\bar{D}} = 5$, $\gamma_{-1} = 5$.

The values of γ_1, H_1 and H_2, same as in Figure 1.

temperature in a zirconium oxide shell of $R_0 - R_{ox}^0 = 0.1$ μm is

$$t_D \cong (R_0 - R_{ox}^0)^2/D_i \cong 4.1 \text{ s}$$

where $D_i = D_i^0 \exp(-E/RT)$, $D_i^0 \cong 0.018$ cm^2/s and $E = 131$ kJ/mole.[40] Thus

$$t_D/t_r \gg 1 \tag{32}$$

and this ratio increases with the temperature. The "initial temperature" at which condition (Eq. 32) is satisfied, is usually much higher than room temperature. Our model assumes that the particle attains instantaneously this initial temperature. This simplifying assumption significantly reduces the number of the parameters in the model and drastically decreases the effort involved in the analysis and presentation. The impact of this simplification will be the subject of a future publication. On the other hand, the assumption that the temperature is uniform inside the entire pellet is valid as

$$t_r \gg t_{therm} \tag{33}$$

For example, the characteristic thermal diffusion time $t_{therm} \cong R_0^2/\kappa$, for a *Zr* particle[41] with $R_0 = 5$ μm is $\cong 2.5 \times 10^{-9}$ s., which is significantly smaller than that of the reaction.

The model assumes that oxygen adsorption and decomposition generate electrical charge carriers and oxygen ions on the particle surface, while initially no charge carrier and electric potential exist. The equilibrium surface concentrations of these charge carriers depend on the particle temporal temperature and ambient oxygen concentration. The initial heating of the particle causes the surface to undergo a transition from equilibrium at a low temperature and charge concentrations to a nonequilibrium state, at which the oxygen surface adsorption rate largely exceeds that of the desorption (Eq. 5). This, in turn, increases the surface concentrations of the charge carriers. The charge carriers diffuse through the product oxide shell to the shrinking core metal at which they are consumed by a very fast oxidation. Because of the different diffusive fluxes and the high surface concentrations of the two charge carriers, a high voltage forms. Thus, the particle surface and the metal shrinking core serve as a source and sink between which the charge carriers diffuse. The higher the surface concentrations are the larger can be the difference between them and, consequently, the generated voltage. A similar growth in the carrier concentrations and voltage may be achieved by increasing the gaseous oxygen concentration (Eq. 12).

In contrast to previous studies[11-13,15-18,9,10] we do not assume a steady-state balance of charge carriers in the oxide layer, that is, points in the oxide shell need not be locally neutral. The fluxes of charge carriers on the particle surface depend on the fluxes of gaseous oxygen to the particle surface and on the oxygen concentration in the surrounding gas. The initial concentrations of the charged carriers in the oxide shell are assumed to attain nonequilibrium values for the chemical reactions occurring at the initial temperature.

Figures 1a and 1b show that the profiles of the negative and positive charge carriers are essentially identical, except for initially close to the surface. Due to the difference in the diffusion coefficients one charge carrier diffuses faster than the other to the metal core. Consequently, initially the surface concentration of the slow diffusing charge carrier exceeds that of the fast diffusing one. Thus, when the ratio between the positive and negative diffusion coefficient ($\bar{D}$) exceeds unity $n > p$, close to the surface (at $\xi \to 1$, Figure 1a), and the surface potential becomes negative (Figures 2a and 3a at $E_{\bar{D}} > 0$), while the inverse occurs when $\bar{D} < 1$ (see Figures 1b and 3a at $E_{\bar{D}} < 0$). The magnitude of the concentration difference and, consequently, the surface electric charge and potential, increases with $|\bar{D} - 1|$. Therefore, for large positive $E_{\bar{D}}$ and $\bar{D} > 1$, the concentration difference decreases as the initial temperature increases (Figure 1a), while for smaller $E_{\bar{D}}$, so that $\bar{D} < 1$, the inverse occurs (Figure 1b). No electric signal forms when the diffusion coefficients are equal (Figure 3a, $E_{\bar{D}} = 0$). The voltage polarity on a pellet with a thin initial oxide may change due to a variation in the value of $\bar{D}$. The larger the value of $|\bar{D} - 1|$ the stronger is the acceleration of the slower charge carriers (oxygen ions at $\bar{D} > 1$) by the faster moving ones (electron holes at $\bar{D} > 1$), and the shorter is the time of complete metal consumption and that at which the maximum temperature is reached ($\tau|_{\theta_m}$). In contrast, the time at which the maximum surface electric potential is attained ($\tau|_{\phi_m}$) as well as the conversion at the maximum electric potential ($\eta|_{\phi_m}$) increase with $|\bar{D} - 1|$ (Figures 2b and 3b).

The formation of a potential maximum may be explained by a transition from a noncorrelated fast diffusion of one carrier to a much slower co-operative carrier diffusion. Initially, the fast diffusing carriers (electron holes when $\bar{D} > 1$) diffuse into the oxide shell from the pellet surface. This increases the excess of the slower carriers (oxygen ions when $\bar{D} > 1$) and the corresponding electric charge and potential (negative at $\bar{D} > 1$) on the surface. The developing electric field retards the fast diffusing charge carriers and accelerates the slow moving ones. Eventually the high electric field correlates the diffusive fluxes of the two charge carriers. This causes a gradual decrease in both the excess of the slower carriers and the electric potential on the particle surface (see n (1) $-$ p (1) in Figures 8 and 9). The larger $|\bar{D} - 1|$ is higher electric fields (ϕ_m), and longer times are required to establish this co-operative fluxes (Figures 2a and 2b and Figures 3a and 3b). Ignoring the Joule heating by the electrical field ($H_0 = 0$) explains the very small changes in θ_m, $\tau|_{\theta_m}$ and $\eta|_{\theta_m}$ with $\bar{D}$ or $E_{\bar{D}}$ at the same D_- (Figures 2a and 3a). On the other hand, the sharp dependence of $\eta|_{\phi_m}$ on $\bar{D}$ (Figures 2b and 3b) is due to the much faster growth of the initial oxide layer at large $\bar{D}$.

The characteristic time of heat removal exceeds largely that of the reaction. The temperature maximum is achieved after the maximum of the reaction rate has occurred, when the heat lost from the particle is equal to the heat released by the reaction, which is retarded by the slow charge carrier diffusion through the growing product shell. Therefore, increasing the intensity of the heat removal H_1 or H_2 decreases the maximum temperature and causes it to occur earlier (at smaller $\tau|_{\theta_m}$) and at a lower conversion ($\eta|_{\theta_m}$). The heat removal rate is smaller than that of the maximum heat generated by the reaction. Thus, it has a negligible impact on the time when the maximum reaction rate is achieved. Our model predicts that the maximum reaction rate corresponds to the maximum flux of gaseous oxygen (oxygen ions and electron holes) through the oxide

shell and, consequently, to the maximum of the electric potential on the particle surface. Thus, increasing H_1 or H_2 has a minor impact on $\tau|_{\phi_m}$, ϕ_m and $\Delta\phi_m$ (Figures 4 and 5) and it decreases the time delay between $\tau|_{\theta_m}$ and $\tau|_{\phi_m}$ (conversion increment $\eta|_{\theta_m} - \eta|_{\varphi_m}$).

The heat transfer by radiation is about three times larger than the convective one and has a strong nonlinear temperature dependence. Hence, an increase in H_1 decreases θ_m gradually, but increasing H_2 leads to a sharp decrease in θ_m at relatively small values and to a moderate decrease at large H_2 values (Figures. 4 and 5). For example, at $H_2 \to 0$ $\theta_m \cong 1.5$ (Figure 5), and the heat removal rate by radiation is about three times that by convection. At $H_2 \geq 5$, the maximum dimensionless temperature is very close to unity, and the heat removal by radiation is very close to that by convection. A similar dependence of $\eta|_{\theta_m}$ on H_2 is noted in Figure 5.

Increasing the heat-transfer coefficients H_1 and/or H_2, decreases the temperature. When $\bar{D}$ (θ) is independent of the temperature or is a monotonic increasing function of the temperature, increasing H_1 or H_2 increases the combustion time. However, if $\bar{D}$ increases as the temperature decreases then an increase in the rate of heat removal may decrease the total combustion time τ_c. This may occur when τ_c is more sensitive to changes of $\bar{D}$ than of H_1 and H_2.

The surface concentrations of the charge carriers are much smaller than the equilibrium ones before the maximum temperature is attained (Figure 8 and 9). Using Eq. 16, we get as a first approximation of n and p

$$y = \frac{A^2}{4}\left(\left[1 + \frac{4}{A^2} + o(1)\right]^{1/2} - 1\right)^2 \quad \text{at} \quad np^2 \ll \chi \quad (34)$$

Substitution of Eq. 34 into Eqs. 18 and 19 indicates that the charge carriers fluxes depend on the activation energy of the adsorption (see also Eq. 17), but not of the desorption. An increase of the activation energy (smaller A) decreases the carrier fluxes to the metal core, the conversion, the temperature rise rate and the surface electric potential before the maximum electric potential is achieved (Figure 6b). The effect is more pronounced for higher rates of heat removal that decrease the particle temperature. Note that when the maximum reaction rate is obtained a large fraction of the metal is still unconverted and the carrier concentrations at the metal-oxide interface are still much smaller than those at equilibrium.

The carrier surface concentrations closely approach the equilibrium ones ($n(1) \to \chi^{-1/3}$, $p(1) \to \chi^{-1/3}$, Figures 8 and 9) after the maximum temperature has been achieved, and we get from Eq. 16

$$y = 1 - 2\frac{1 - np^2\chi}{1 + 2/A} + o\left(\frac{1 - np^2\chi}{1 + 2/A}\right) \quad \text{at} \quad 1 - np^2\chi \ll 1 \quad (35)$$

In accordance with Eq. 18 and 19 this leads to very small fluxes of the carriers depending on the activation energy of both adsorption and desorption. The difference between the activation energies of the adsorption and desorption determines the equilibrium values, and it affects the carrier concentrations mainly during $\tau > \tau|_{\theta_m}$. When $\gamma_{-1} - \gamma_1 > 0$ $(\gamma_{-1} - \gamma_1 < 0)$ the carrier concentrations are ascending (descending) functions of time while the particle temperature drops (Figures 8 and 9). When $\gamma_{-1} = \gamma_1$, the carrier concentrations tend to be constant and independent of the temperature drop.

The characteristic scale of the electric potential distribution $\Delta\xi$ increases proportionally with the ratio of a characteristic surface molar flux of oxygen ions to the maximum possible oxygen flux to the pellet surface, β. This decreases correspondingly the spatial gradients of ϕ, and the impact on the diffusion fluxes on the particle surface (Eq. 18 and 19). The temporal temperature and $\eta|_{\theta_m}$ behavior barely changes as β does. The flux of ions near the metallic core and the oxidation rate Eq. 28 or τ_c, are also insensitive to changes in β (Figure 10). On the other hand, the carrier concentrations and electric potentials on the surface (Eq. 25) decrease with an increase in β (Figure 10).

Our calculations (Figure 6 and 7) predict that the electric voltage is generated mainly after the reaction rate attained its maximum and before the temperature reached its maximum The time of voltage duration is about 10^{-2} of the combustion time. In our calculations, the characteristic scale of the electric potential, (see Eq. 20), is 0.13V at 1,500 K. The calculations shown in Figures 2 and 3 predict a potential of about 0.5 V for a typical pellet. These predictions are in a good agreement with experimental results[6,42].

Conclusions

Our model explains and predicts the generation of a temporal electrical potential during the nonisothermal oxidation of a single metal pellet. It assumes that the rate of the chemical reaction can be described by the shrinking-core model. Oxygen ions and electron holes are generated on the particle surface and diffuse through the growing oxide shell to the metal core, at which they are consumed by a very fast reaction. The pellet surface and the shrinking metal core surface act as a source and sink of the charge carriers, while the oxide shell separates the charges. The different rates of diffusion of the positive and negative charge carriers through the oxide shell generate an electric potential. The ratio between the diffusion coefficients of the charge carriers determines the surface electric potential amplitude, polarization, and the difference between the time the particle potential and temperature attain their maximums. The larger is the ratio between the diffusion coefficients, the greater is the voltage, and the smaller is combustion time, as well as the difference between the time, the particle potential and temperature attain their maximums. As this difference can be readily measured, it offers a critical test of the validity of the model.

The larger the convective and/or radiation heat transfer coefficients are the shorter is the difference between the time the surface electric potential and the temperature attain their maximum values. At sufficiently high rates of heat removal from the particle both the potential and temperature attain their maximum values at essentially the same time. Owing to the temperature dependence of the diffusion coefficients the time of total metal consumption may decrease with increasing rate of heat removal, that is, larger heat transfer coefficients. On the other hand, the amplitudes of the surface electric potential and potential difference across the oxide shell decrease with an increase in the rate of heat removal at a large ratio of the two diffusion coefficients.

The activation energies of adsorption and desorption have different impact on the pellet temporal temperature and surface potential behavior. During the initial oxidation stage, before the temperature has reached its maximum an increase in the activation energy of the adsorption strongly decreases the rates of the temperature rise, the oxidation and of the surface electric potential formation at sufficiently large values of the heat transfer coefficients. The activation energy of the oxygen desorption and the difference between the activation energies of desorption and adsorption affect mainly the behavior after the maximum temperature has been attained. The larger is the desorption activation energy, the longer is the duration of the temperature and potential decrease during the later combustion stage.

The equilibrium carrier concentrations for each temperature are determined by the difference between the activation energies of adsorption and desorption. The surface carrier concentrations attain the equilibrium values by the time of the maximum temperature has been achieved. The carrier concentrations within the particle and at the metal-oxide interface attain the equilibrium much later.

When the rate of heat removal is low a sharp drop in the electric potential amplitude is caused by an increase in the ratio between the characteristic molar flux of oxygen ions from the surface and the maximum possible flux of oxygen to the pellet surface. However, this increase almost does not influence the maximum combustion temperature and combustion time, as well as the time at which the surface electric potential reaches its maximum.

Acknowledgments

We are grateful to the NSF, CRDF and the Materials Research Science and Engineering Center at the University of Houston for financial support of this work. We also wish to thank Dr. S. I. Doronin for help in the numerical calculations.

Notation

A = dimensionless oxygen adsorption rate, defined by Eq. 17
A_0 = dimensionless adsorption pre-exponent, defined by Eq. 17
C = specific heat capacity, $J/(kg \cdot K)$
$\bar{D}$ = ratio of carriers diffusion coefficients, defined by Eq. 20
D_i = diffusion coefficients, m^2/s
E_i = activation energy J / $mole$
$E_{\bar{D}}$ = dimensionless activation energy of $\bar{D}$
e = electron/electron charge, C
h = electron hole
H_0 = dimensionless Joule heating coefficient, defined by Eq. 30
H_1 = dimensionless convective heat transfer coefficient, defined by Eq. 30
H_2 = dimensionless radiative heat transfer coefficient, defined by Eq. 30
ΔH = heat of reaction, J/m^3
I = dimensionless maximum surface oxygen flux, defined by Eq.(28).
k = Boltzmann constant, J/K
k_i, k'_j = reaction rate constants in Eqs. 2 and 3
$\tilde{k}_i$ = dimensionless rate constant, defined by Eq. 13
k = thermal diffusivity, m^2/s
k_c = mass-transfer coefficient, m/s
M_W = molecular weight, $kg/mole$
n = dimensionless oxygen ions concentration, defined by Eq.17
N_A = Avogadro number
p = dimensionless concentration of electron holes, defined by Eq. 17
r = radial coordinate, m
R = universal gas constant, $J/(K \cdot mole)$
R_0 = external radius of spherical pellet, m
R_{ox} = shrinking metal core radius, m
T = temperature, K
t = time, s
t_r = characteristic time of intrinsic metal oxidation, s
t_{therm} = characteristic time of thermal diffusion, s
t_D = characteristic time of oxygen ion diffusion, s
W_i = surface reaction rate, $mole/(m^2 s)$
V_O^{++} = oxygen vacancy
y = dimensionless oxygen concentration, defined by Eq.17

Greek letters

α = heat transfer coefficient, $J/(m^2 \cdot s \cdot K)$
β = dimensionless oxygen ions molar surface flux, defined by Eq. 20.
γ_1 = dimensionless adsorption activation energy, defined by Eq. 17.
γ_{-1} = dimensionless desorption activation energy, defined by Eq. 17.
ε = emissivity
η = conversion
ϕ = dimensionless electric potential, defined by Eq. 20.
φ = electric potential, V
Λ = dimensionless Debye screening length, defined by Eq. 21.
ν = stoichiometric index
θ = dimensionless temperature, defined by Eq. 17.
ρ_{cond} = condensed phase density, kg/m^3
σ_{el} = electric conductivity, $1/(\Omega \cdot m)$
σ = Stefan-Boltzmann constant, $J/(m^2 \cdot s \cdot K^4)$
τ = dimensionless time, defined by Eq. 23
ξ = dimensionless radial coordinate, defined by Eq. 20.
χ = dimensionless ratio of reaction rate constants, defined by Eq. 17.

Subscripts and superscripts

ads = adsorbed
c = metal consumption time
g = gaseous
m = maximum values
ox = at the metal-oxide interface
0 = initial value
00 = ambient temperature
1 = surface
i = interface
$\times$ = lattice
$*$ = equilibrium concentrations
$-/+$ = electric charge of defects
∞ = ambient concentration

Literature Cited

1. Nersesyan MD, Claycomb JR, Ming Q, Miller JH, Richardson JT, Luss D. Chemomagnetic fields produced by solid combustion reaction. *Appl Phys Lett*. 1999;75,8:1170-1172.
2. Claycomb JR., LeGrand W, Miller Jr. JH, Nersesyan MD, Ritchie JT, Luss D. Chemomagnetic characterization of chemical reactions using high-T_c SQUIDs. *Phisica C*. 2000;341**:**2641-2644.
3. Nersesyan MD, Claycomb JR, Ritchie JT, Miller J.H., Richardson J.T., Luss D. Electric and magnetic fields generated by SHS *J Mater Synth and Process*. 2001;9,2:63-72.
4. Nersesyan M.D., Luss D., Claycomb J.R., Ritchie J.T., Miller Jr. J.H. Magnetic Fields produced by the combustion of metals in oxygen. *Combust Sci and Tech*. 2001;169**:**89-106.
5. Nersesyan M.D., Ritchie J.T., Filimonov I.A., Richardson J.T., Luss D. Electric fields produced by high-temperature metal oxidation. *J of the Electrochem Soc*. 2002; 149,1:J11–J17.
6. Martirosyan K.S., Filimonov I.A., Nersesyan M.D., Luss D. Electric field formation during combustion of single metal particles. *J of the Electrochem Soc*. 2003:150,5:J9–J16.
7. Kofstad P. *High Temperature Corrosion*. London and NY: Elsevier, 1988.
8. Gellings P.J., Bouwmeester H.J.M. *The CRC Handbook of Solid State Electrochemistry*. Boca Raton - New York - London - Tokyo: CRC Press, 1997.
9. Rode H., Hlavacek V., Viljoen H.J., Gatica G.E. Combustion of

metallic powders: A phenomenological model for the initiation of combustion. *Combust Sci and Tech.* 1992;88:153-175.
10. Rode H., Orlicki D., Hlavacek, V. Reaction rate modeling in non-catalytic gas-solid systems: Species transport and mechanical stress. *AIChE J.* 1995;41,12:2614-2624.
11. Wagner C. Uber den Zusammenhang zwischen Ionenbeweglichkeit and Diffusionsgeschwindigkeit in festen Salzen. *Z Phys Chem.* 1930; B11**:**139-151 (in German).
12. Wagner C. Beitrag zur Theorie des Anlaufvorgangs. *Z Physik Chem.* 1933;B21**:**25-41 (in German).
13. Wagner C. Equations for transport in solid oxides and sulfides of transition metals. *Progr Solid State Chem.* 1975;10(1):3-16.
14. Cabrera N., Mott N.F. Theory of the oxidation of metals. *Rept Progr Phys.* 1949;12**:**163-184.
15. Fromhold AT. *Theory of metal oxidation (Defects in crystalline solids)*. Vol. 1. Amsterdam - New York - Oxford: North-Holland Pub. Co., 1976.
16. Fromhold AT. *Theory of metal oxidation (Defects in solids)*. Vol. 2. Amsterdam - New York - Oxford: North-Holland Pub. Co., 1980.
17. Fromm E. *Non-Stoichiometric Compounds, Surfaces, Grain Boundaries and Structural Defects*. NY: Kluwer, 1989.
18. Kapila D, Plawsky JL. Solid-state film diffusion for the production of integrated optical waveguides. *AIChE J.* 1993;39**:**1186-1195.
19. Merzhanov AG, Mkrtchyan SO, Nersesyan MD, Avakyan PB, Martirosyan KS. Magnetic Field Caused by SHS process. *Dokladi Akad Nauk RA*. 1992; **93**, 2:81-83.
20. Avakyan PB, Nersesyan MD, Merzhanov AG. New materials for electronic engineering. *Amer Ceram Sos Bull*. 1996;75,2:50-55.
21. Kudryashov VA, Mukasyan AS, Filimonov IA. Chemoionization waves in heterogeneous combustion processes. *J Mater Synth and Process*. 1996;4,5:353-358.
22. Morozov Yu G, Kuznetsov MV, Nersesyan MD, Merzhanov A.G. Electrochemical Phenomena in the Processes of the SHS. *Dokladi Akademii Nauk Rossii*. 1997;351,6:780-782.
23. Maksimov Yu M, Kirdyashkin AI, Korogodov VS, Polyakov VL. Generation and transfer of an electric charge in self-propagating high-temperature synthesis using the Co-S System as an Example. *Combust Explos Shock Waves.* 2000;36,5:670-673.
24. Martirosyan KS, Filimonov IA, Luss D. Self-heating by joule dissipation during gas-solid combustion reactions. *Intern J SHS*. 2003;12,2: 91-98.
25. Filimonov IA, Luss D. Electrical field formation during the oxidation of a metal particle. *AIChE J*. 2004;50,9:2287-2296.
26. Wen CY. Noncatalytic heterogeneous solid fluid reaction models. *Industrial and Engineering Chemistry*. 1968; **60**, 9:34-54.
27. Levenspiel O. *Chemical Reaction Engineering*. NY: John Wiley, 1972.
28. Dou S, Masson CR, Pacey PD. Mechanism of oxygen permeation through lime-stabilized zirconia. *J Electrochem Soc*. 1985;132**:**1843-1849.
29. Ramanarayanan TA, Ling S, Anderson MP. Electrochemical analysis of mixed conduction in ceramic oxide membranes. *Proc. of the 2nd Intern. Symp. On Solid Oxide Fuel Cells*, Athens, Greece, 1991:777-786.
30. Lin Y-S, Wang W, Han J. Oxygen permeation through thin mixed-conducting solid oxide membranes. *AIChE J*. 1994;40,5:786-798.
31. Chandra S. *Superionic solids. Principles and applications.* Amsterdam - New York - Oxford: North-Holland Pub. Co., 1981:101-117.
32. Jerome JW. Consistency of semiconductor modeling: an existence/stability analysis for the stationary van roosbroek system. *SIAM J Appl Math*. 1985;45,4:565-591.
33. Barcilon V, Chen D-P, Eisenberg RS, Jerome JW. Qualitative properties of steady-state Poisson-Nernst-Planck systems: perturbation and simulation study. *SIAM J. Appl Math*. 1997;57,3:631-648.
34. Park J.-H., Jerome J.W. Qualitative properties of steady-state Poisson-Nernst-Planck systems: mathematical study. *SIAM J Appl Math*. 1997; 57,3:609-630.
35. Press W.H., Flannery B.P., Teukolsky S.A., Vetterling W.T. *Numerical Recipes in C: The Art of Scientific Computing*. Cambridge University Press, 2nd ed., 1993.
36. Crank J., Nicholson P. *Proc. Cambridge Philos. Soc.* 1947;43**:**50-67. [Re-published in: John Crank 80th birthday special issue. *Adv Comput Math.* 1997;6**:**207-226].
37. Thomas L.H. *Elliptic problems in linear difference equations over a network*. Watson Sci. Comput. Lab. Rept., Columbia University, New York, 1949.
38. Ames W.F. *Numerical Methods for Partial Differential Equations*. 2nd Ed. New York: Academic Press, 1977.
39. Manning PS, Sirman DS, DeSouza RA, Kilner JA. The kinetics of oxygen transport in 9.5 mol % single crystal yttria stabilized zirconia. *Solid State Ionics*. 1997;100**:**1-2.
40. Shelby J.E. *Handbook of Gas Diffusion in Solids and Melts*. Materials Park, OH: ASM International, 1996.
41. Grigoriev IS, Melikhov EZ. *Handbook of Physical Quantities*. New York: CRC Press, 1997.
42. Martirosyan K.S., Filimonov I.A., Luss D. Electric field generation by gas-solid combustion. *AIChE J*. 2004;50,1:241-248.

Manuscript received Apr. 24, 2004 and revision received Aug. 28, 2004.